Chapter 3

Atomic Mechanisms Governing Strength of Metallic Nanosized Crystals

Sergiy Kotrechko, Olexandr Ovsijannikov,
Igor Mikhailovskij and Nataliya Stetsenko

Additional information is available at the end of the chapter

http://dx.doi.org/10.5772/intechopen.75159

Abstract

Fundamentals of the atomic mechanisms governing the strength of nanosized metallic crystals are described. An attempt is made to explain on this basis the size and orientation effects, temperature dependence of strength and atomism of fracture of bcc crystals under triaxial uniform (hydrostatic) tension. A feature of the proposed material is that it combines the results of molecular dynamics simulation with the data of experimental research findings on failure of metallic nanosized crystals under the high-field mechanical loading. It is exhibited that local instability of the lattice is the main mechanism governing the strength of defect-free nanosized crystals (NSC). Based on the concept of local instability, an explanation is given of the nature of the size effect in NSC, as well as of the differences in its manifestation in nanocrystals with bcc and fcc lattices. The concept of the mechanism of thermal activation of local instability is outlined. This enables to explain the specific features of the temperature dependence of NSC. The results of experimental studies and molecular dynamics simulation of the failure of tungsten nanocrystals under hydrostatic tension are presented. The ideas about the atomism of the bcc-fcc transition in these conditions are articulated.

Keywords: molecular dynamic simulation, nanosized crystals, lattice instability, strength, nanowire, size effect, surface tension

1. Introduction

Significant advances in the fabrication of nanoscale objects with controlled size and properties (nanorods, nanowires, nanopillars and carbyne chains) are a characteristic feature of nanotechnology development in the last decade. In turn, this stimulates the development of experimental

methods for characterising the properties of these nanoobjects, as well as computer methods for predicting their behaviour under various external influences. Nanosized metallic crystals occupy a special place among these objects. Due to their remarkable physical and mechanical properties, they can be directly used in various nanodevices; in addition, they are considered as building blocks for the creation of nanocrystalline materials. On the other hand, study of nanosized crystals enables to ascertain the fundamental mechanisms of deformation and fracture inherent in the nanoscale. Fabrication of defect-free nanocrystals and their compression test [1–3], as well as the development of a high-field technique for the preparation and *in-situ* tensile testing of nanoneedles [4–6], becomes a milestone event in experimental studies of nanosized crystals. Absence of defects (dislocations and twins) in these crystals made it possible to reach extremely high levels of strength, which are close to the value of "theoretical strength". Therefore, molecular dynamics (MD) simulation is the most effective tool for studying atomic mechanisms to reach extremely high levels of strength in crystals.

Nanosized crystals of bcc metals are a classical object of MD simulation [7–13]. Currently, considerable attention is paid to metals with a bcc lattice [14–20]. From a physical point of view, bcc metals are more interesting because they provide a greater variety of atomic rearrangements, governing the strength. However, the main difficulty in MD simulation of bcc metal is lack of sufficiently reliable potentials, which limits the accuracy of such simulation. In this connection, the appearance of direct experimental data on the strength of bcc nanocrystals substantially facilitated the problem of selection and verification of these potentials. A great number of works on MD-simulation enabled to predict the key effects controlling the level of strength of nanosized nanocrystals, namely: (i) the size effect, (ii) dependence of strength on orientation, (iii) the temperature dependence of strength, and (iv) dependence of strength on the stress state mode [7–24]. At the same time, the absence of a completed theory of strength of nanosized crystals is a characteristic feature of science of the strength of these objects. Lack of sufficient experimental data is the second feature of state-of-the-art in researches of strength of nanosized crystals. Difficulties in performing mechanical tests of nanospecimens are the reason for this. In this regard, the high-field mechanical tests of nanosized specimens should be indicated. It has made it possible *in situ* mechanical loading of nanosized specimens up to level close to theoretical strength combined with direct observation of the atomic structure of these objects under well-controlled crystallographic conditions [25, 26].

In the present work, fundamentals of the atomic mechanisms governing strength of nanosized metallic crystals are described; besides, an attempt is made to explain on this basis the size and orientation effects, temperature dependence of strength, and atomism of fracture of bcc crystals under triaxial uniform (hydrostatic) tension.

2. Methods of physical and numerical experiments

2.1. Field-induced mechanical test

The *in situ* mechanical loading of nanosized crystals in the FIM experiments was realised using the Maxwell mechanical stress induced by high electric fields. As was shown in these studies,

the vast majority of dislocations was removed under the action of the electric field–induced mechanical stresses. So, most of the dislocation-free nanosized crystals were fractured at mechanical stresses corresponded to substantial parts of the ideal strength of solids. This technique was used for uniaxial tensile tests of tungsten and molybdenum nanoneedles and for uniform triaxial (hydrostatic) tensile tests of a tungsten nanocrystal.

The intrinsic hydrostatic tensile strength of tungsten was experimentally determined using a high-field testing in field-ion microscope (FIM) with needle-shaped specimens (**Figure 1a**) [6]. The specimens with an initial radius of curvature of about 100 nm and the taper angle of $5-15^{\circ}$ were etching in a NaOH solution of 99.98% pure tungsten wires with the <110> texture. The specimen surface was preliminary polished by low-temperature field evaporation [25]. Field ion images were acquired at the voltage of 4–22 kV. For mechanical loading, a high voltage pulse V_p with duration of 20 ns was applied. The local field at specimen surface was determined as

$$F = \frac{F_0 \times (V_0 + V_p)}{V_0}, \tag{1}$$

where V_0 is the applied voltage corresponding to the threshold field for evaporation F_0 [25, 27]. The evaporation field of tungsten F_0 on the [110] facets at 77 K is 57 V nm^{-1} related to an evaporation rate of ~10^{-2} atomic layers per second. The electric field decreases severely under

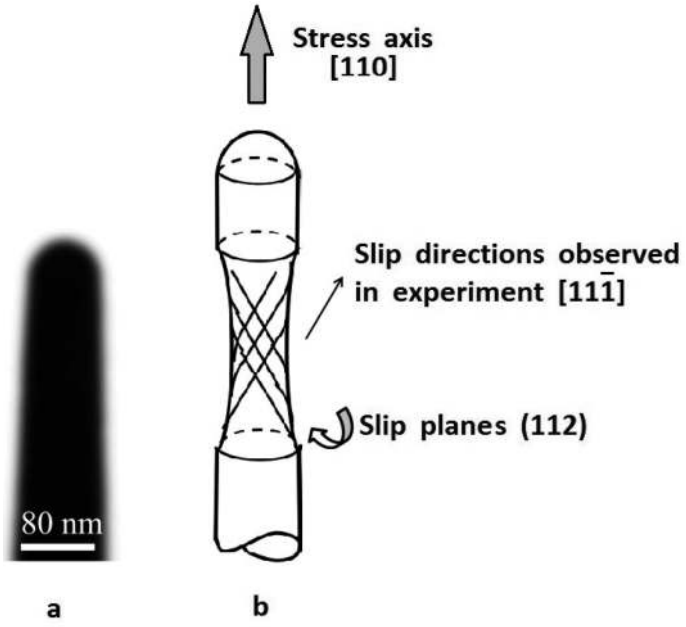

Figure 1. An electron microscopic image of Mo nanotip formed by field evaporation (a) and the sketch of a high-field tension test (b).

the hemispherical cap in the conical part. So, the failure of needle-shaped specimens was usually initiated at the nanosized cap in the region of the ultimate field strength. An electric field applied to a metal specimen induces the Maxwell surface stress

$$\sigma_s = \frac{\varepsilon_0 F^2}{2} \tag{2}$$

where ε_0 is the electric constant. This stress acts normal to the surface element at all points. The stress state of a needle-shaped specimen is possible to estimate to any plane in the specimen apex section by integration of the stress components at each point on the surface. The Maxwell stress acting over the metal surface produces the force in the axis direction is given by:

$$f_z = \frac{1}{2}\iint \varepsilon_0 F^2 \cos\beta dS, \tag{3}$$

where dS is an element of surface area, β is the angle between the axis and the normal to that surface facet. The integral is taken over the whole specimen surface. The local Maxwell stress is calculated by integration of the field-induced stress and dividing by the area of the section concerned. The near surface Maxwell stress under the hemispherical envelope of the specimen is virtually hydrostatic and equals to the local surface stress determined by Eq. (3). The stress state in the conical shank region is corresponded to the tensile test with uniaxial tension. It enables both to deform nanocrystal plastically and to break it under uniaxial tension (**Figure 1b**).

For nanocrystal failure under multiaxial uniform (hydrostatic) tension, a protrusion was formed on the spherical part of specimen. It was created by selection of special schedules for the high-field evaporation of atoms from the nanospecimen surface [19]. This is shown schematically in **Figure 2a**. Electric field strength and, accordingly, mechanical stresses increase with decrease in the curvature radius of a surface. So, maximal stresses act in this protrusion. This makes it possible to fracture the metal exactly in this volume. It is done by a steep increase in the electric field strength. Appearance of the crater on a nanoneedle surface is the direct evidence that fracture *occurs* in the local region, where hydrostatic tension acts (**Figure 2b**).

The Maxwell stress was determined with accuracy of ±4%. The systematic error due to uncertainties in the field calibration is ±3% (see [28, 29]), and, correspondingly, the systematic error in determination of the Maxwell stress is ±6%. The total error in determination of the Maxwell stress is ±10%.

2.2. Molecular dynamics simulation

To analyse atomic mechanisms of instability and failure of defect-free nanosized crystal under uniform triaxial (hydrostatic) tension, MD simulation was employed. Simulation was performed using the software (program package) XMD [http://xmd.sourceforge.net/].

Extended Finnis–Sinclair semiempirical potential [30] (**Tables 1** and **2**) was utilised for MD simulation of hydrostatic tension of tungsten. This potential overcomes the "soft" behaviour of the original Finnis–Sinclair potential [31].

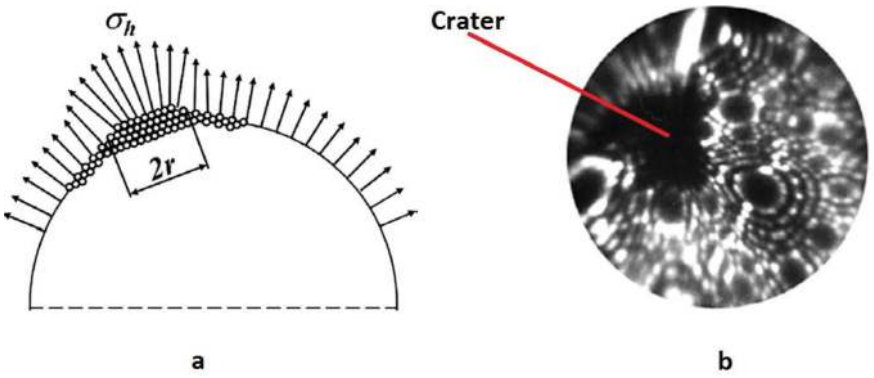

Figure 2. The schemes of the nanoneedle tip and loading (r is the protrusion radius) *before failure* (a) and FIM microfractograms of tungsten nanotip acquired at 5.60 kV *immediately after failure* (b).

A, (eV A^{-1})	d, A	c, (A)	c_0, (eV A^{-2})	c_1, (eV A^{-3})	c_2, (eV A^{-4})	c_3, (eV A^{-5})	c_4, (eV A^{-6})
1.885948	4.41	3.25	48.527 96	−33.79621	5.854334	−0.0098221	0.033338

Table 1. Potential parameters for W.

A, (eV A^{-1})	d, A	c, (A)	c_0, (eV A^{-2})	c_1, (eV A^{-3})	c_2, (eV A^{-4})	c_3, (eV A^{-5})	c_4, (eV A^{-6})
1.848648	4.1472	3.2572	47.98066	−34.09924	5.832293	0.017494	0.020393

Table 2. Potential parameters for Mo.

According to EAM or FS formalism, the total energy of a system is given by the expression:

$$U_{tot} = \frac{1}{2}\sum_{ij} V(r_{ij}) + \sum_{i} f(\rho_i) \tag{4}$$

where the first term is the conventional central pair-potential summation:

$$V(r) = \begin{cases} (r-c)^2(c_0 + c_1 r + c_2 r^2 + c_3 r^3 + c_4 r^4), & r \le c \\ 0, & r > c \end{cases}$$

and the second term is the n-body term:

$$f(\rho_i) = \sqrt{\rho_i} \quad \rho_i = \sum_{i \neq j} A^2 \varphi(r_{ij})$$

$$\varphi(r) = \begin{cases} (r-d)^2, & r \le d \\ 0, & r > d \end{cases}$$

Uniform triaxial tension of ball-shaped nanosized tungsten crystal was also simulated. Initial radius of nanocrystal was 10.8 nm. Such a size enabled to eliminate the influence of rigid surface shell on the behaviour of atoms in the inner region of specimen. To describe the distribution of atomic velocities for given temperature, the Boltzmann distribution was used. To hold simulated temperatures, velocity of atoms was scaled by $(T_t/T_c)^{1/33}$ (T_t is the value of temperature kept during simulation; T_c is the instantaneous system temperature at each time step). To avoid a shock wave when loading, gradient velocity is added to interior atoms [32]. Thermal motion of the atoms of the surface layer of a thickness 0.5 nm was "frozen." These atoms had only the radial component of the velocity, which ensured uniform triaxial expansion of the ball shell with the rate 5 m/s. Accordingly, the strain rate was 4.63×10^8 s^{-1}. Tension of nanowires of molybdenum and tungsten in three crystallographic directions [100], [110] and [111] was modelled also. Cylinder with the axis oriented along a corresponding crystallographic direction was cut from the set of atoms placed exactly at a lattice site. Relation between the diameter and the length of cylinder is one-quarter. After that, boundary conditions are applied. The central part (gauge length) of the cylinder with length of 3 diameters is still free, but atoms of border parts are made "frozen." Time step is 10^{-15} sec. The diameter of nanospecimens varied within the range 1÷13 nm. In addition, to interpret the experimental data on the destruction of nanopillars under uniaxial compression, MD simulation of the compression of cylindrical Mo specimens in the [100] direction was performed.

For the quantitative analysis of the driving forces of atomic rearrangements, in addition to global stresses σ_{ij} (average over the specimen), local ξ_{ij} stresses (acting within the volume per atom) were estimated. The local stresses ξ_{ij} were determined as:

$$\xi_{ij}^k = \frac{1}{2\Omega^k} \sum_{m(\neq k)}^{n} f_i^{km} r_j^{km}. \tag{5}$$

where k refers to the considered atom; m refers to the neighbouring atom; f_i^{km} is the force vector between atoms k and m determined as the gradient of energy functional; r_j^{km} is the position vector between atoms k and m; n is the number of the nearest neighbouring atoms; Ω^k is the atomic volume; and i, j are the stress tensor indexes.

An expression for the global stresses σ_{ij} is the following:

$$\sigma_{ij} = \frac{1}{N} \sum_{k=1}^{N} \xi_{ij}^k. \tag{6}$$

where N is the total number of atoms in the nanowire.

For calculation of the local shear stresses, the following formula was used:

$$\xi_{ns} = \sum_{i,j} \xi_{ij} n_i s_j \tag{7}$$

where n_i is the normal vector for the glide plane, s_j is the slip direction.

True strain value was employed as a measure of longitudinal strain of the nanowire as a whole:

$$e_{xx} = \ln\left(1 + \frac{\Delta l_{xx}}{l_0}\right) \tag{8}$$

where l_0 and Δl_{xx} are the initial gauge length of a specimen and its increment, respectively.

When modelling hydrostatic tension of a nanosized ball-shape specimen, engineering strain value was determined as:

$$e = \frac{\Delta r}{r_0} \tag{9}$$

where r_0 and Δr are the initial values of radius of ball and its increment, respectively.

3. Results and discussion

As it is known, microscopic defects (dislocations and twins) are the main reason for decrease in strength of materials. Modern nanotechnologies enable us to create materials, which, in most cases, are defect-free. Therefore, initially, it was believed that their strength must tend to the ideal strength and be the intrinsic material trait much like the elastic constants. However, it was appeared that the strength of nanosized crystals changes within the wide range depending on their sizes, temperature, loading condition, etc. However, the concept of "ideal strength" can be used as a starting point for the analysis of *atomic mechanisms* governing the strength of nanosized crystals. The ideal strength of a material is defined to be the maximal *homogenous* stress that an ideal crystal can withstand. Reaching of the limit state of such crystal is related to uniform and simultaneous break of atomic bonds or its reformation. In general case, two instability modes exist for metals, namely (i) instability of crystal under the tensile stresses (instability on the Bain path for bcc crystals) and (ii) shear instability. The first mode of instability of an ideal crystal results in its disintegration. Shear instability gives rise to change in shape and orientation of an ideal crystal [33–35].

A fundamental difference of nanosized crystals from the ideal ones is that the nanocrystals can be defect-free but not ideal since the ideal position of atoms in the crystal lattice is disturbed by both (i) action of surface tension forces and (ii) thermal vibrations of atoms. Action of the surface tension forces leads to inhomogeneous distribution of local stresses. Thermal vibration of atoms causes local stress fluctuations. These two factors are the main reasons for *localisation* of process of breaking and reformation of atomic bonds in nanosized crystals [36, 37]. As a result, the above two modes of an ideal lattice instability occur in a nanosized crystal, but this instability is realised in a limited local region of the crystal. This gives rise to the fact that defects form as a result of above instability. For instance, formation of dislocations and twins is a direct consequence of this localised shear instability. The key difference of these defects from those in macrosized single crystals lies in the fact that they are *highly* non-equilibrium, since they are formed in a defect-free crystal at stresses much exceeding the critical stress of their

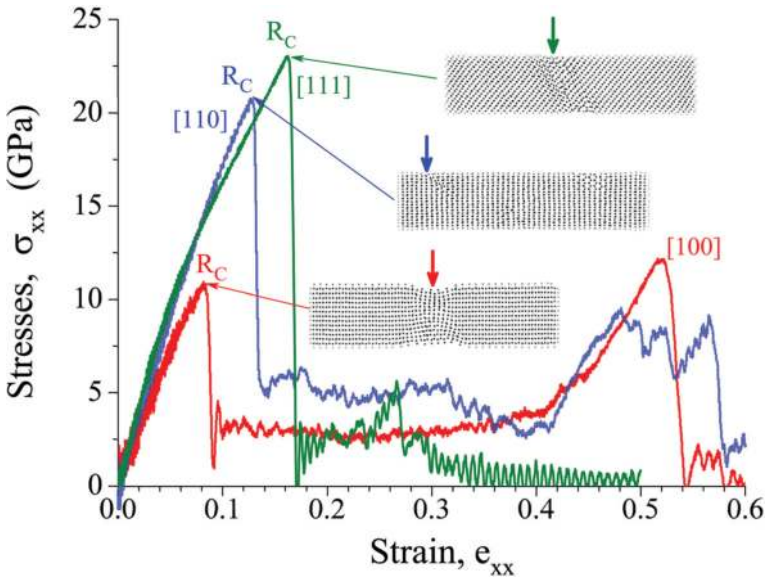

Figure 3. Images of Fe-nanowires and diagrams of their strain at temperature 300K for three crystallographic orientations: arrows indicate instability regions; R_C is the instability stress (strength of nanowire).

propagation in a crystal (**Figure 3**). As shown in **Figure 3**, the stress of formation for these defects predetermines the level of strength of nanosized crystals [37].

3.1. The effect of surface

A characteristic feature of nanosized objects is the significant influence of the surface on their properties. For mechanical properties, the surface effect is realised through the surface tension. As it is known, in nanosized specimens, the level of stresses created by surface tension may reach significant values even without loading [8]. Surface tension forces induce tensile stresses in the surface layer of the crystal, which are balanced by compressive stresses in the bulk. It gives rise to *inhomogeneous* local stress distribution within interior of the nanosized specimen. **Figure 4** presents the cross-sectional distribution of local shear stresses $\xi_{ns,}$ which act in shear systems, where instability of crystal is observed. According to these data, even in the case of the unloaded nanowire, the value of shear stresses in a surface layer of Mo nanowire may reach values of the order of 4 GPa. This is only 3 times less than theoretical shear stress for Mo. At loading of such specimen, these stresses cause the lattice instability in sub-surface layer (**Figure 4d**). Surface tension not only gives rise to localization of the instability region in surface layer, but it is also the reason for size effect, which manifests itself in growth or decrease in strength of nanosized crystals (**Figure 5**). Recently, two approaches exist to explain

http://dx.doi.org/10.5772/intechopen.75159

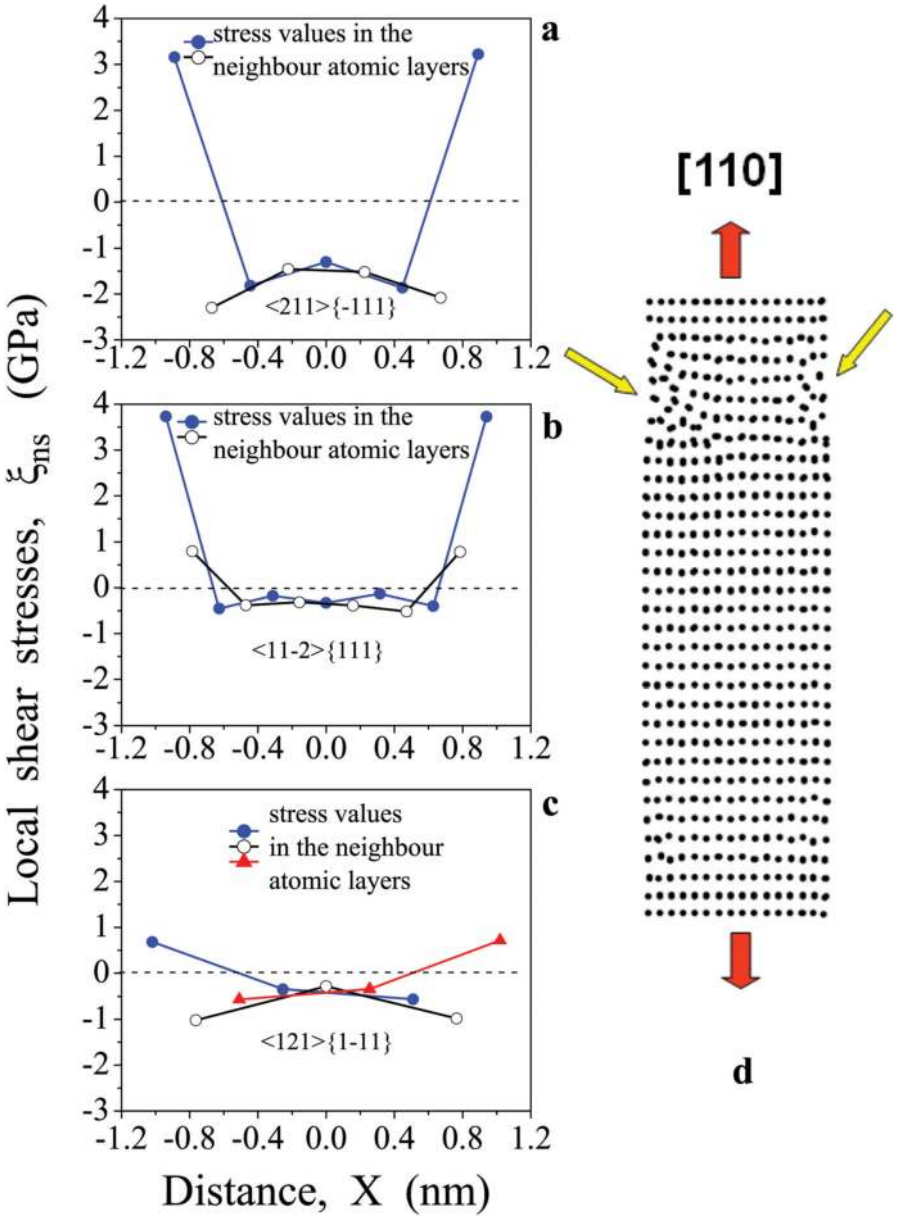

Figure 4. Distribution of the local shear stresses ξ_{ns} in the slip systems <211>{−111}, <11-2>{111} and <121>{1-11} for unloaded Mo nanowires in directions [100] - (a), [110] - (b), and [111] - (c) at T = 0 K. The cross-section diameter is 2.1 nm; (d) localisation of lattice instability in surface layers.

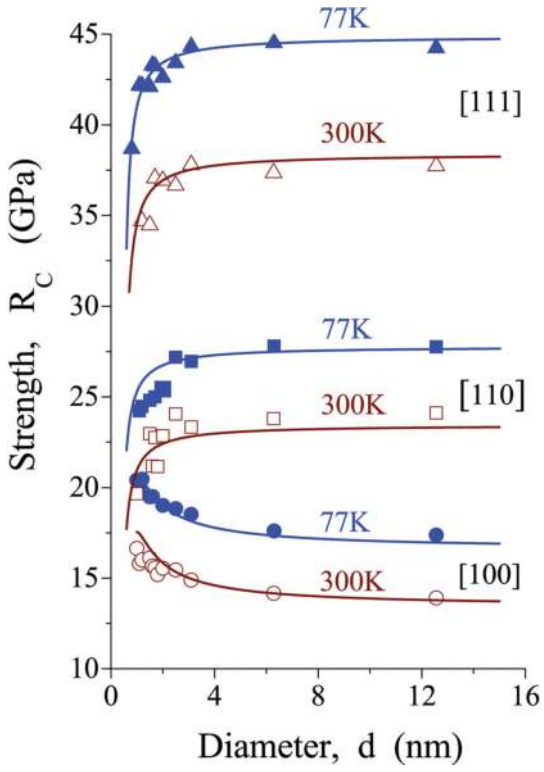

Figure 5. Dependence of strength of Mo nanowire on its diameter at T = 77K and T = 300 K for three crystallographic orientations: points are the results of MD simulation; solid lines are calculations by (12) for the following orientations (with corresponding values of parameters):[110] (f_{xx} = 1.777 n/m, h = 0.29 nm, m = 0.470, τ_c = 15.9 GPa (T = 77 K), τ_c = 13.9 GPa (T = 300 K), α = 1);[111] (f_{xx} = 2.345 n/m, h = 0.40 nm, m = 0.314, τ_c = 15.9 GPa (T = 77 K), τ_c = 13.9 GPa (T = 300 K), α = 1);[100] (f_{xx} = 2.070 n/m, h = 0.10 nm, h^* = 0.40 nm, m = 0.47, τ_c = 9.7 GPa (T = 77 K), τ_c = 8.3 GPa (T = 300 K), α = 1).

size effect. The first of them is based on a "global" criterion of limit state [8, 10, 16], and the second one employs the "local" criterion of nanocrystal instability [14, 15, 18, 19].

Because of the surface tension, an inner part of a nanosized crystal is compressed, and the thin surface region is stretched. If thickness of this stretched layer is neglected, then compressive stresses σ_{xx}^{in} in the inner part of specimen may be estimated as:

$$\sigma_{xx}^{in} = -\frac{4f_{xx}}{d} \tag{10}$$

where f_{xx} is the surface tension along the specimen axis, and d is the diameter of specimen.

Global approach supposes that at compression of a nanosized specimen, stress σ_{xx}^{in} is "added" to applied stress, which gives rise to decrease in the global stress required for transition from elastic to plastic strains, i.e., to decrease its strength. According to (10), the value of σ_{xx}^{in} should

increase with reduction of a specimen diameter. At tension, the effect of a specimen diameter on the strength must be inverse, i.e., the value of R_C must increase with the diameter growth. This agrees with findings of MD simulation of tension and compression of nanowires with fcc lattice [7–10, 36]. According to the MD simulation finding on tension of nanowires made of fcc metals (Cu, Ni, Au, Ag), at a cross-sectional dimension less than 4.0 nm, there is an increase by 10–20% of their strength level with a decrease in the cross-sectional dimension. It should be emphasised that this effect is observed for orientations [100], [110], and [111] in fcc nanowires and in nanowires of bcc metals at orientations [100] [7–10, 12, 16, 36, 37]. At the same time, it was shown in [37] that an opposite effect is observed under tension in the [110] direction of Mo nanowires. In this case, the strength of nanowire decreases with decreasing its diameter. A similar effect was ascertained for Fe nanowires [17]. MD simulation of the Mo nanowire carried out in this paper shows that for Mo, analogous regularities are also observed for [111] orientation (**Figure 5**). This difference in the behaviour of fcc and bcc nanowires cannot be explained within the framework of existing global approach. Based on the results of MD simulation and direct experimental data, it was shown in [4, 14] that under uniaxial tension, the failure of metal nanowires is governed by shear instability, the result of which is the formation of non-equilibrium dislocations or twins in the surface layer. Such a mechanism of failure is observed even in bcc nanowires at low temperatures. Therefore, in the proposed local approach, the instability criterion can be written in terms of *local* shear stresses ξ_{ns}, as:

$$\xi_{ns} \geq \tau_c \tag{11}$$

where τ_c is the critical stress of local instability of crystal in a surface layer.

To derive the criterion of nanocrystals instability within the framework of continuum approach, the concept of "effective" thickness h of surface layer can be used. This is the thickness of a layer where the distribution of effective shear stresses ξ_{ns}^{sf} is homogeneous, but their effect on strength is the same as in the case of real inhomogeneous stress distribution. In this case:

$$\xi_{ns}^{sf} = m\sigma_{xx}^{sf} = \frac{mf_{xx}d}{\alpha h(d-h)} \tag{12}$$

where d is the diameter of specimen; m is the orientation factor for system where shear instability occurs; α is the coefficient taking into account biaxial stress state on the nanospecimen surface ($\alpha \geq 1$); and σ_{xx}^{sf} is the effective tensile stress, which acts in the subsurface layer. Therefore, the value of effective compressive stress σ_{xx}^{in} acting in internal volume of specimen is:

$$\sigma_{xx}^{in} = -\frac{4f_{xx}d}{(d-2h)^2} \tag{13}$$

Using the criterion (10) with (11) gives the first approximation for strength R_C:

$$R_C \approx \frac{\tau_c}{m} - \frac{f_{xx}d}{\alpha h(d-h)} \tag{14}$$

According to this dependence, at $d >> h$, the surface tension must give rise to decrease in strength R_C, but the degree of this decrease does not depend on specimen diameter. At small

values of d (in our case at $d \leq 4 \div 5$ nm), reduction of d must result in growth of ξ_{ns}^{sf}, and, respectively, decrease in R_C. This agrees well with the results of MD simulation of tension in directions [110] and [111] (**Figure 5**). At tension in these crystallographic directions, local instability results in formation of non-equilibrium dislocation. Layer width, necessary to form this dislocation, is of the order of the Burgers vector. This is comparable with the width of stretched sub-surface layer of nanospecimen, and so, surface tension facilitates its formation. At tension of bcc nanosized crystals in the direction [100], the local instability is due to formation of non-equilibrium twin [16]. To form this kind of defect, the greater crystal volume is needed; so, the region of the crystal, where twin forms, is located in the site where the compressive stresses act. This reduces the magnitude of the resulting shear stress acting at the time of defect formation. As a result of this, the level of applied stresses necessary for the instability of a nanospecimen, i.e., its strength, increases. In this case, the upper estimate for the nanowire strength is:

$$R_C \approx \frac{\tau_c}{m} - \frac{f_{xx} d}{\alpha h (1+\beta)(d-h)} + \frac{4\beta f_{xx} d}{\alpha (1+\beta)(d-2h)^2} \tag{15}$$

$$\text{where } \beta \approx \frac{h^*}{h}\left[1 - \frac{h+h^*}{d-h}\right] \tag{16}$$

h^* is the thickness of the layer within which the defect is affected by oppositely directed shear stresses; β characterises the ratio of the slip plane areas located within the regions of compressive and tensile stresses.

The third term in this dependence accounts for the effect of decrease in total value of shear stresses influencing the twin, which is due to the fact that part of twin is located in a compressed region. As it is exhibited in **Figure 5**, dependence (15) enables to describe the effect of increase in strength at tension in the direction [100]. Thus, this rather simple model enables to explain not only the anomaly of the size effect at tension of nanowires of bcc metals in the <100> directions but also the difference between the regularities of size effect in fcc and bcc metals. For all three orientations <100>, <110>, and <111>, local instability in fcc metals is due to formation of a non-equilibrium stacking fault, the critical size of which exceeds a thickness of a tensile surface layer. As a result, for these three crystallographic orientations, the effect of increase in R_C at decrease in a specimen diameter is observed. In bcc metals, the same effect is observed only at tension in directions <100>, when twin forms. At tension in directions <110> and <111>, the inverse effect is observed, because local instability results in formation of non-equilibrium dislocations. Therefore, differences in regularities of manifestation of size effect in bcc and fcc metals are due to different kinds of defects, which form as a result of local instability of a crystal. Thus, dependence of the magnitude of the local shear stresses in the surface layer of nanowire on its diameter is the reason for the existence of a size effect for the strength of nanowires. The "sign" of this effect (increase or decrease in strength with decreasing diameter) is determined by the kind of non-equilibrium defect, which is formed as a result of local instability of the nanocrystal. When a non-equilibrium twin (bcc nanowire: orientation <100>) or a stacking fault (fcc nanowires: orientations <100>, <110>, and < 111>) is formed, the strength of the nanowire increases with decreasing its diameter. Formation of a non-equilibrium

dislocation (bcc nanowires: orientations <110> and < 111>) gives rise to the opposite effect—a reduction in strength with a reduction in the diameter of the nanowire.

3.2. The temperature effect

As noted above, there are two main reasons for localisation of the lattice instability in nanocrystals, namely: (i) the effect of surface tension and (ii) the local stress fluctuation due to oscillations of atoms in the lattice. Statistical distribution of local shear stresses in nanosized crystal of iron at two temperatures is exhibited on **Figure 6**. Limit state of a nanosized crystal is reached when the local shear stresses ξ_{ns} attain the critical stress of local instability τ_c. In general case, τ_c is the critical stress, at reaching of which the highly non-equilibrium dislocation or twin forms in crystal. The value of a fluctuation component of local shear stresses $\delta\xi_{ns}$ depends on temperature. As shown in **Figure 6**, it leads to temperature dependence of the strength R_C.

The fluctuation component $\delta\xi_{ns}$ can be presented as:

$$\delta\xi_{ns} = t\sqrt{D_\xi(T)} \tag{17}$$

where D_ξ is the value of variance of local shear stresses in a subsurface layer, where dislocation or twin forms; t is the dimensionless characteristic of the fluctuation value. Its magnitude depends on the probability of occurrence of such fluctuation. According to the criterion of

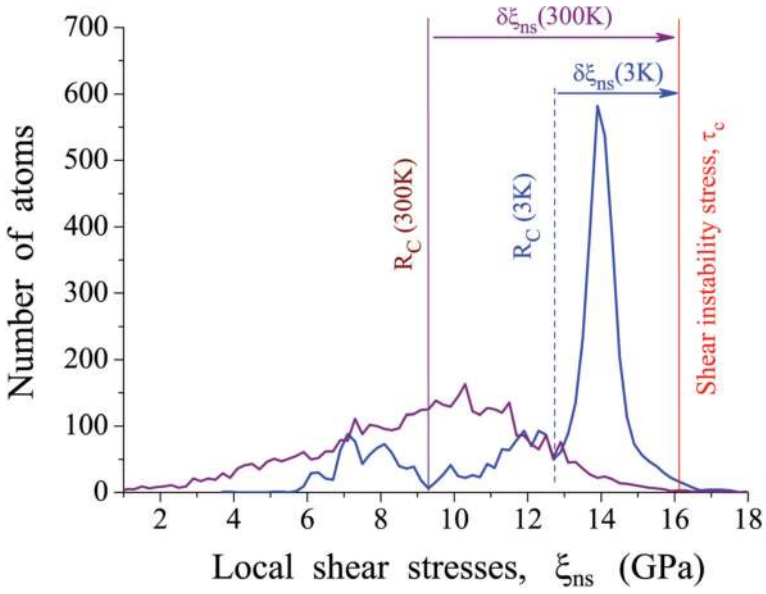

Figure 6. Distributions of local shear stresses ξ_{ns} (in the slip system ([1 $\bar{1}$ $\bar{1}$](211)) for instability point R_C in Fe–nanowire under uniaxial tension in [100] direction at T = 3 K and T = 300 K [37].

local instability (10) and expression (16), the first approximation for the temperature dependence of nanosized strength R_{un} may be presented as:

$$R_{un} \approx \frac{\left[\tau_c - \xi_{ns}^{sf} - t\sqrt{D_\xi(T)}\right]}{m} \tag{18}$$

Thus, temperature dependence of the local stress fluctuations $\delta\xi_{ns}$ (16) gives the main contribution to the temperature dependence of the strength of nanosized crystals. From the Debye model [38] and results of computer simulation [39], it follows that within the range of temperatures, greater than the Debye temperature (θ_D), the variance of atomic displacements is linear function of temperature, and for lower temperatures, susceptibility D_ξ to change in temperature decreases. In [18], experimental evidence was first obtained for the temperature dependence of Mo nanosized specimens (**Figure 7**). From these data, it follows that at temperatures higher than θ_D, the expression (18) gives the correct qualitative description of the temperature dependence of the strength of nanosized crystals, if assume the linear dependence of D_ξ on T. It should be noted that the nature of the strength temperature dependence for nanosized crystals and macrosized single crystals differs essentially because, in first case, thermal vibration of atoms

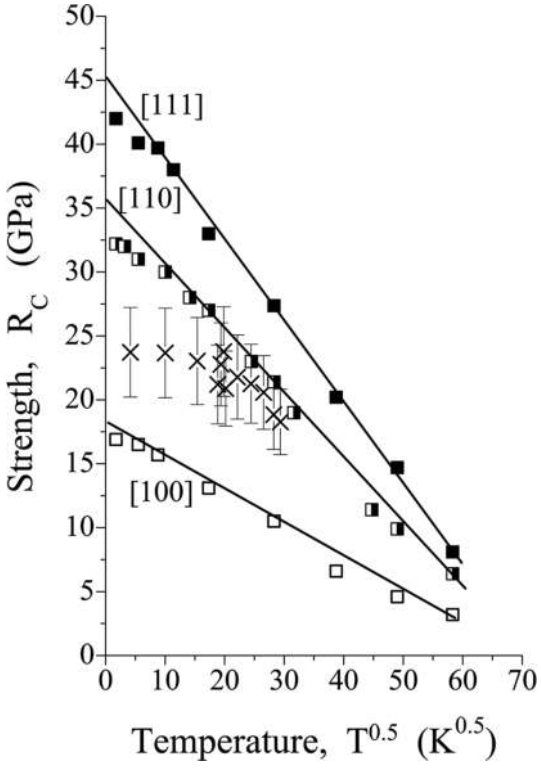

Figure 7. Dependence of strength of nanosized W crystals on the temperature and crystallographic direction: ■, ◨, □ are the results of MD-simulation, ✕ are the experimental evidence [18].

causes local instability in defect-free structure and *nucleation* of defects. In the second case, the lattice vibration facilitates *mobility* of already existent defects. It is necessary to emphasise the fundamental difference in the mechanisms and structural levels of realisation of these processes. In the first case, we are talking about the thermal activation of instability of the crystal lattice (atomic-scale event). In the second case, the oscillation of the dislocation line (a microscopic object) plays a key role, leading to the formation of kinks pairs, by means of which a thermally activated overcoming by dislocation of the potential relief occurs. As a result, the laws of temperature dependence differ as well as change in the absolute strength value. For instance, over the temperature range 77K…300K, the value of yield strength of typical bcc transition metals decreases 3–5 times, while the changes of a critical stress of NSC instability do not exceed 15–25%.

3.3. Nanosized crystal instability under hydrostatic tension

As noted above, there are two modes of crystal instability, namely shear instability and instability under the action of tensile stresses. In ideal bcc crystals, this is manifested in the existence of instability on the orthorhombic deformation path and instability on the Bain path. As mentioned above, a shear instability in nanowires is usually realised at tension in directions <110> and <111>. In the general case, when the bcc crystals are stretched in the <100> direction, *ab-initio* computation predicts the possibility of instability, both on the orthorhombic and Bain paths. As a result, the mode of instability is realised, for which a lower value of strains is required. So, for example, for an ideal niobium crystal, the value of critical strain of instability on the orthorhombic path is almost 1.5 times less than the corresponding strain on the Bain path [34]. This means that the strength of Nb nanowires at tension in the direction <100> should be governed by local shear instability. The situation with Mo, W, and Fe is more complicated. According to the results of *ab-initio* calculations, for ideal crystals of these metals, the values of critical strains and stresses on both paths are very close [33–35]. However, the results of the MD simulation on tension of nanowires of these metals indicate the realisation of local shear instability. One of the results of such instability is the reorientation of the crystal lattice from [100] to [110]. According to the *ab-initio* calculations, such a reorientation should be a consequence of the instability on the orthorhombic path. The only difference is that in an ideal crystal, this reorientation must occur simultaneously in the entire crystal, and in a nanosized specimen, this occurs locally with subsequent propagation to the entire volume of nanospecimen (**Figure 8**). These regularities were considered in the works [14, 40]. Later, similar results were obtained on nanowires with a square cross-section [16]. As a result of realisation of the shear instability mechanism at tension of Mo, W, and α-Fe nanowires in the direction [100], brittle fracture (Bain instability) does not occur, but on the contrary, the plastic strain is larger as compared with that for orientations [110] and [111] [14, 40]. In this connection, the question arises whether it is possible to realise instability on the Bain path in *nanosized* specimens made of the bcc metals. Bain instability was found in [14] at MD-simulation of hydrostatic tension of ball-shaped specimen of iron. Under hydrostatic tension, the value of the average shear stresses is zero. This contributes to the realisation of the Bain instability, since there is no driving force for the shear instability of the crystal. However, the bcc→fcc transition requires the realisation of a certain relationship between the strains of lattice along the

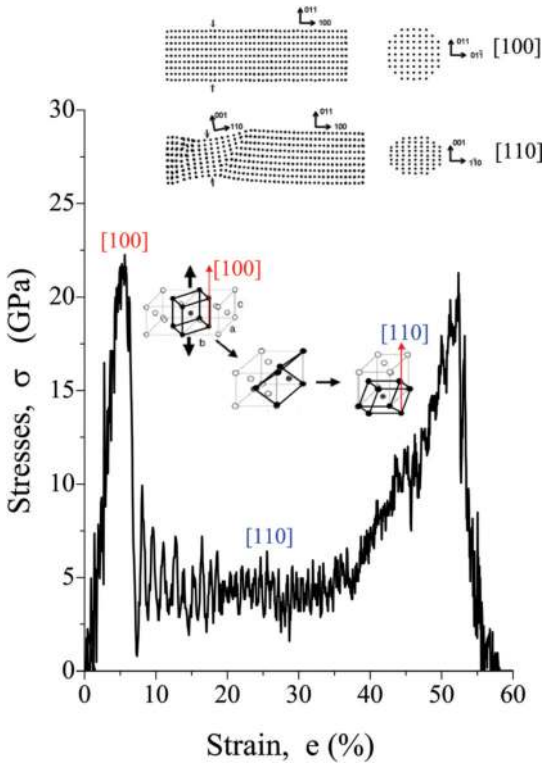

Figure 8. Stress-strain dependence for Mo nanowire. Uniaxial tension in the direction [100] at T = 30 K, and schemes of the lattice re-arrangement.

directions OX, OY, and OZ [34]. This is impossible to be realised under conditions of *uniform* triaxial tension. To analyse the details of this mechanism of bcc→fcc transition in nanosized crystals, hydrostatic tension of a molybdenum nanoball with a diameter of 10.8 nm was simulated [19]. MD simulations were performed for T = 77 K (the temperature for which the experimental data were obtained) and also for a lower temperature of 30 K. Simulation at lower temperatures makes it possible to obtain a clearer picture of atomic rearrangements, since thermal "smearing" of atom locations is reduced. Based on the results of this simulation, the diagram of deformation of the ball was built (**Figure 9**). To analyse local bcc-fcc rearrangements, for each atom, the number of neighbouring atoms in the first coordination sphere was calculated. This permits to determine the regions in crystal with both initial bcc lattice and formed unstable fcc lattice, as well as heavily deformed regions (**Figure 9**).

According to the MD-simulation findings, when critical stress of instability of a specimen under uniform triaxial tension, R_C, is reached, displacements of atoms in the specimen are essentially non-uniform (**Figure 9**). Bands form in the specimen, and deformation of the lattice in them differs from the deformation in the other part of the specimen. Detailed analysis of atomic rearrangements showed that global instability of entire specimen is initiated by bcc→fcc

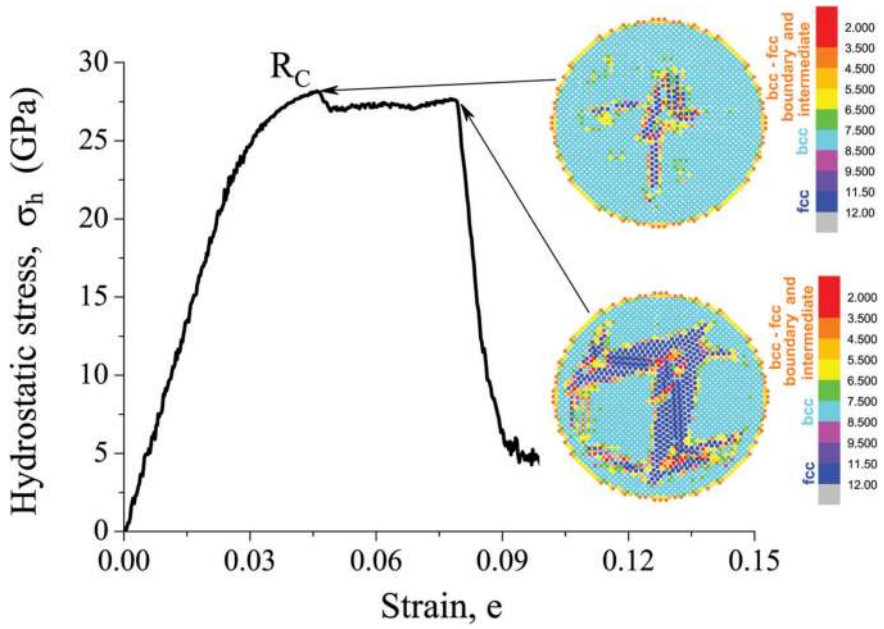

Figure 9. Diagram of deformation of the ball-shaped Mo nanosized specimen under hydrostatic tension at T = 30 K and crystallographic structure of the ball-shaped nanosized specimen at the moment of its instability and at the moment of crack initiation. The colour range indicates the number of atoms in the first coordination sphere for the selected atom.

transition within the local regions, i.e., instability on the Bain path is realised in these regions. At further loading of a specimen, the regions with such type of a lattice expand and new regions with fcc lattice may form as well. **Figure 9** demonstrates by different colours the atoms belonging to bcc and fcc lattices, atoms forming the boundaries between these regions, and atoms from the regions with strongly non-uniform distribution of atomic displacements (read colour).

To analyse quantitatively the instability initiation for the temperature 77K, distribution of local tensile stresses $\xi_{\{100\}}$, acting on planes {100} at the moment of instability of nanosized specimen, was built (**Figure 10**). According to these data, significant fluctuation of the local stresses $\xi_{\{100\}}$ is observed. This gives rise to change in local stresses over the wide range of values—from 10.6 GPa to 40.8 GPa at the average value of 28 GPa. The local maximum on the left branch of distribution appears due to rigid surface shell, which is necessary to realise uniform tension of specimen. According to the evidence obtained, Bain instability is initiated at the value of local stresses $\xi_{cm} \approx 40$ GPa. This stress exceeds significantly that for bcc→fcc transition at purely *uniaxial* tension $\sigma_{ct} = 28.9$ GPa [41]. Action of tensile stresses in the direction normal to that, in which Bain instability realises, is the reason for above excess. Findings of *ab-initio* calculations for iron presented in [42] show that when applying a tensile stresses in the orthogonal direction, the Bain instability stress increases as compared to purely uniaxial tension. In our case, the Bain transition occurs in one of the directions <100> as a result of *fluctuation* of *local* tensile stress in this direction. This is the feature of the atomic mechanism of

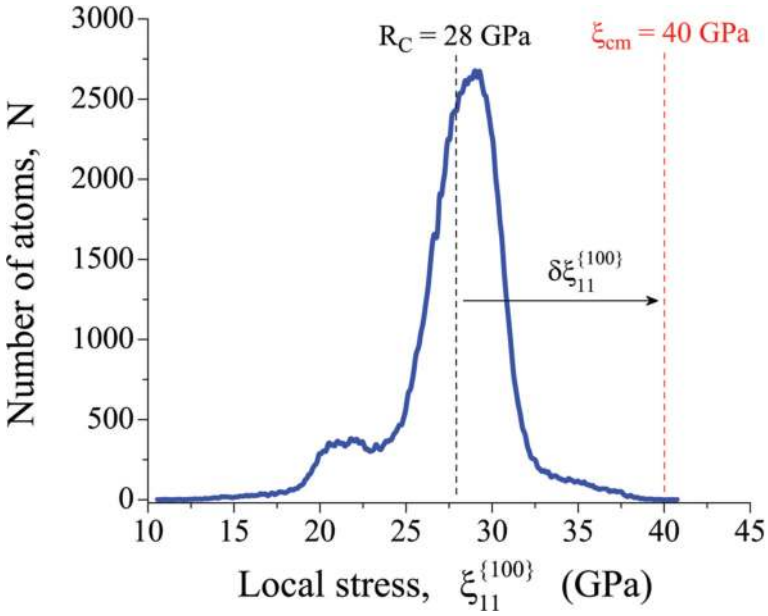

Figure 10. Distribution of local normal stresses $\xi_{11}^{\{100\}}$ in the ball-shaped nanosized specimen at the moment of it instability at $T = 77$ K: R_C is the global stress of instability of the ball-shaped nanosized specimen; ξ_{cm} is local critical stress of bcc → fcc transition; $\delta\xi_{11}^{\{100\}}$ is local stress fluctuation on {100} planes, required for realisation of the local instability of crystal.

instability initiation in nanosized specimen under global uniform triaxial tension. It should be emphasised that in this case, the appearance of fluctuations gives rise not only to excess of the local stresses over the average ones but also to deviation from uniform triaxial tension within the *local region* where the Bain transition is realised.

For quantitative estimates, the expression for value of local stress of Bain transition, ξ_{cm}, under multiaxial stress state, can be written as follows:

$$\xi_{cm} = \overline{E} e_{cm} + \nu(\xi_{YY} + \xi_{ZZ}) \tag{19}$$

where e_{cm} is the critical strain of the Bain transition under multiaxial tension; $\overline{E}$ is the secant modulus; ν is the Poisson's ratio; ξ_{YY} and ξ_{ZZ} are the local orthogonal tensile stresses.

The probability of *simultaneous* fluctuations of local stresses in three mutually orthogonal directions is many orders of magnitude less than probability of fluctuation in *only one* direction, so, in the first approximation, at the moment of local instability:

$$\xi_{YY} \approx \xi_{ZZ} \approx R_C \tag{20}$$

where R_C is the global (average) tensile stress at the moment of initiation of nanosized crystal instability.

Respectively:

$$\xi_{cm} \approx \overline{E} e_{cm} + 2\nu R_C \tag{21}$$

Dependence (20) enables to estimate the value of local stress of initiation of local instability, ξ_{cm}, at a given value of global stress R_C. In this case, the experimental value of the global stress of instability of a ball-shape nanospecimen $R_C = 28 \pm 3$ GPa [19] (**Figure 11**). Assuming that e_{cm} is approximately equal to critical strain of the Bain transition at uniaxial tension ($e_{cm} \approx 0.12$ [41]); and $\overline{E} \approx 0.5E_{\{100\}}$ [19], where $E_{\{100\}}$ = 409 GPa is elasticity modulus of tungsten and $\nu = 0.27$, one obtains ξ_{cm} = 40.3 GPa.

To estimate ξ_{cm}, the value of critical strain of initiation of Bain transition at pure uniaxial tension was used. According to the data of *ab-initio* calculations, the value of critical strain of the lattice instability increases at transition from uniaxial to triaxial tension, and at uniform triaxial tension, it reaches maximum value of 0.15 [42]. It means that obtained value ξ_{cm} = 40.3 GPa should be considered as the low estimation of critical stress of Bain transition of tungsten at multiaxial tension. In spite of this, the calculated value of ξ_{cm} agrees sufficiently with the value of ξ_{cm} obtained from the analysis of distribution of local stresses in ball-shaped specimen (**Figure 10**).

According *ab-initio* calculation findings, the instability stress of an ideal Mo crystal under uniform triaxial tension is 50.0–52.0 GPa [42]. However, such a value of strength can be reached only in an ideal crystal but not in nanosized specimens. Fluctuations in local tensile stresses are the reason for this. They do not enable the uniform triaxial tension in *local* regions of the crystal to be

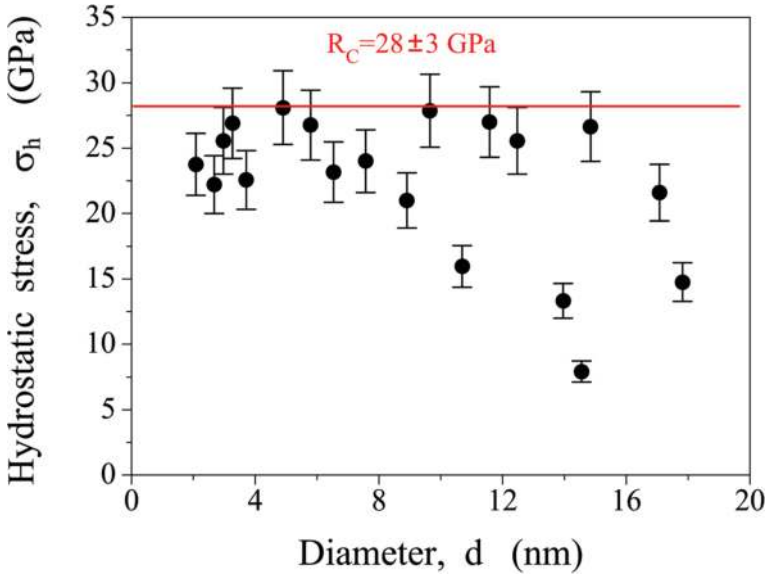

Figure 11. Hydrostatic tensile strength of tungsten nanocrystals at 77 K; d is the diameter of nanocrystal region fractured under hydrostatic tension; R_C is the experimental evidence of strength.

realised at a *global* (on average) *uniform* triaxial tension of the entire specimen. Probability of the fluctuation of local stresses in three directions simultaneously is much lower than the probability of fluctuation along one of the directions <100>; so, initiation of instability of nanosized tungsten crystal occurs at local stresses $\xi_{cm} \approx 40$ GPa. This means that in local regions, the instability occurs at non-uniform triaxial tension ($\xi_{11} \approx 40$ GPa; $\xi_{22} \approx \xi_{33} \approx 28$ GPa).

Thus, the strength of nanosized crystals under hydrostatic tension will always be below the strength of an ideal crystal under the same conditions. In this case, the strength of tungsten nanosized crystals under hydrostatic tension is 28 GPa. This is approximately 1.90 times less than the strength of an ideal tungsten crystal. The reason for this is fluctuations of local tensile stresses, which leads to: (i) exceeding of the value of local stresses over global (fluctuations themselves) and (ii) to deviation from triaxial uniform tension within *the local region* where this transition realises. For nanosized Mo specimens, the first factor results in a decrease in strength by 1.43 times, while the second one—by 1.25–1.30 times.

3.4. Strength of nanopillars and nanoneedles

Nowadays, nanoneedles and nanopillars are the most common nanosized specimens, which strength can be determined experimentally. Two main kinds of nanopillars exist, namely: (i) nanopillars obtained by focused ion beam (FIB) technology [43, 44], and (ii) nanopillars obtained by etching of nanocomposites [3]. Surface layer of specimens obtained by FIB technique contains a great number of defects in sub-surface layer, and so their strength does not exceed 1.0–1.5 GPa [43]. The second kind of specimens has no such shortcomings, and so, their strength is much higher. For instance, strength of Mo nanopillars of diameter 300–1000 nm is approximately 9 GPa. This is 6 times greater than strength of nanopillars obtained by FIB technique. However, this strength value is more than 2 times less than the evidence on MD-simulation of compression of defect-free Mo nanopillars of this crystallographic orientation [100]; according to our data, this value is ≈ 20 GPa. This difference can be caused by buckling instability, since at compression tests of nanopillars, it is quite difficult to provide the ideal conditions of uniaxial compression.

A high-field technique of tensile testing *in-situ* of nanoneedles is free of such disadvantage. In addition, it makes it possible to test the specimens of significantly smaller diameters—from 20 till 125 nm. Data presented in **Figure 12** enable to estimate experimentally strength of Mo and W nanocrystals by the value of upper scatter limit of experimental evidence on failure of nanoneedle specimens. This value for W is 23.2 GPa, and for Mo, it is 20.0 GPa. These figures also present the results of MD simulation of tension of cylindrical specimens in the direction [110]. Calculated strength values are approximately 1.4 times greater than the maximum experimental values of the nanopillars strength. At high-field treatment of the tip of nanoneedle specimen, its working volume is "cleaned" from dislocations [4, 19], and so, both decrease the values of strength of nanoneedle specimens, and their scatter may be because of stress raising related to rough lateral surface, which is formed by electrochemical polishing. The results obtained make it possible to identify the main factors leading to a decrease in the strength of nanosized crystals. According to these data, tensile strength of defect-free nanowires is always less than ideal strength. This is due to both surface tension effect (effect of a physical surface) and thermally induced local stress fluctuation (temperature effect). At transition to nanoneedles,

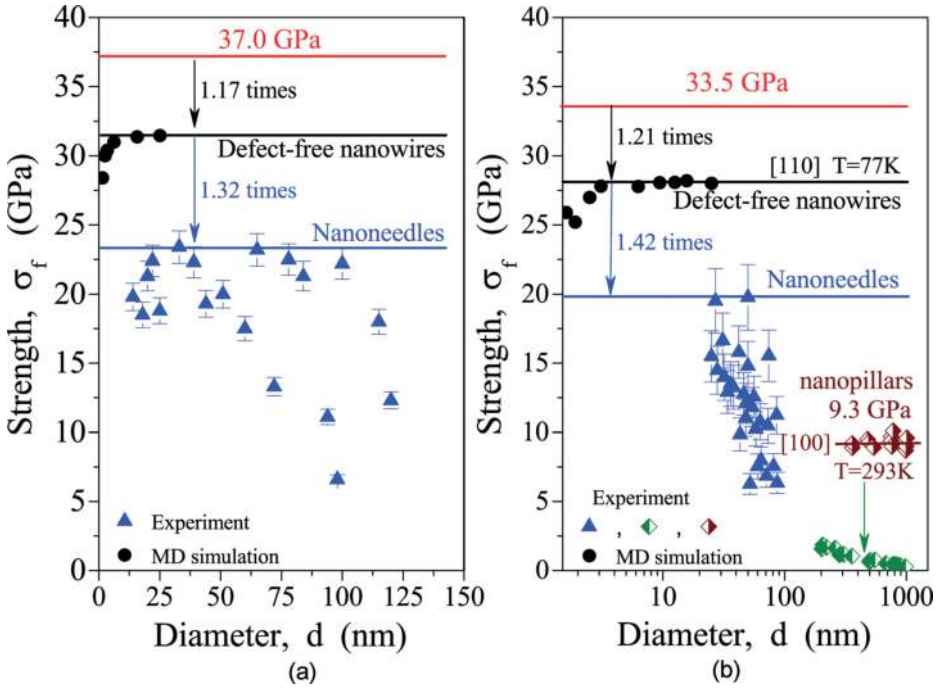

Figure 12. Size effect for nanowires, nanoneedles and nanopillars: W (a) and Mo (b); ◆ are nanopillars manufactured (prepared) by FIB technology (built by the evidence of [43]); ◆ are obtained by etching (built by the evidence of [3]).

we have additional effect of a surface roughness. This effect may give rise to a reduction in strength by at least 30–40%, and it is the cause for considerable scatter of experimental data. The strength of nanopillars is significantly influenced by the buckling effect.

4. Conclusions

1. On the atomic scale, the strength of nanosized crystals (NSC) is governed by two modes of lattice instability. This is instability with respect to the action of tensile stresses and shear instability. In nanosized crystals of fcc metals, the second mode of instability predominates. BCC metals are characterised by a competition between these two modes of instability, depending on the loading conditions of the crystal. Instability on the Bain path is realised at uniform triaxial (hydrostatic) tension. At uniaxial tension, even under cryogenic conditions, the strength of the bcc nanocrystals is controlled by shear instability (instability on the orthorhombic path).

2. Localisation of instability in a limited volume of a nanospecimen is the distinguishing feature of the mechanism of nanosized crystal instability. It occurs due to two main factors: (i) local stresses fluctuation caused by thermal vibrations of atoms and (ii) the effect of

surface tension in NSC. The first factor governs regularities of strength dependence on temperature and the feature of the bcc→fcc transition under hydrostatic tension. The second one influences the absolute value of nanocrystal strength and determines the main regularities in manifestation of the size effect in nanospecimens of bcc and fcc metals, as well as the orientation dependence of the size effect in nanospecimens of bcc metals.

3. Dependence of the magnitude of local shear stresses in the surface layer of nanospecimen, induced by the surface tension, on its diameter (cross-sectional size) is the reason for existence of a size effect for the strength of nanospecimens. The "sign" of a size effect (increase or decrease in strength with decreasing diameter) is determined by the kind of non-equilibrium defect that is formed as a result of local instability of the nanocrystal.

4. Strength of nanospecimen (nanowire) increases with decrease in its diameter (cross-sectional size) if the value of this strength is controlled by the formation of a stacking fault (fcc lattice, orientations <100>, <110>, <111>) or a twin (bcc lattice, <100>). Formation of non-equilibrium dislocations (bcc lattice, <110>, <111>) gives rise to an anomaly of the scale effect, i.e., to fall in strength with decreasing diameter. This is due to the fact that non-equilibrium dislocations form in a thin surface layer, where the action of surface tension gives rise to an increase in the level of local shear stresses, i.e., promotes realisation of the local instability. Size of the region required for the formation of a non-equilibrium stacking fault or twin exceeds thickness of the stretched surface layer, and this region falls within the range of compressive stresses. The latter reduces the magnitude of the resulting local shear stresses in the region where a twin or a stacking fault is formed, which leads to an increase in the strength of nanospecimen.

5. Physical mechanisms of the thermally activated reduction in strength of nanosized and macrosized crystals are fundamentally different. In first case, the thermal vibration of atoms causes local instability in defect-free structure and *formation* of non-equilibrium defects. In the second case, the atom vibrations raise *mobility* of already existent defects. As a result, the laws of temperature dependence differ as well as change in the absolute value of strength. For instance, over the temperature range 77K…300K, the value of yield strength of typical bcc transition metals decreases 3–5 times, while the changes in a strength of nanosized crystals do not exceed 15–25%.

6. Instability in bcc nanocrystals on the Bain path is possible under uniform triaxial tension of nanosized specimens. The peculiarity of the manifestation of "localised instability" under these conditions is that the fluctuations of local tensile stresses not only lead to a decrease in the global (average) stress required for the bcc→fcc transition but also cause deviation from triaxial uniform tension within *the local region* where this transition realises. It means that at a global uniform triaxial tension of nanospecimen, locally, bcc→fcc transition occurs under non-uniform triaxial tension. This leads to a decrease in the magnitude of stress required for such a transition. For W at T = 77 K, this decrease is 25–30%.

The maximum attainable experimental values of the strength of Mo and W nanoneedle specimens in the crystallographic direction [110] are approximately 40% less than the results of MD simulation. This may be caused by stress raising due to rough lateral surface of nanoneedle specimens

forming as a result of electrochemical polishing. This means that formation of an atomically smooth surface of nanoneedles is one of the factors to reach the ultimate strength levels.

Conflict of interest

The authors declare that they have no competing interests.

Funding

This work was supported by the National Academy of Sciences of Ukraine [grants number #0117 U002131; #0117 U006351].

Author details

Sergiy Kotrechko[1]*, Olexandr Ovsijannikov[1], Igor Mikhailovskij[2] and Nataliya Stetsenko[1]

*Address all correspondence to: serkotr@gmail.com

1 G. V. Kurdyumov Institute for Metal Physics, NASU, Kyiv, Ukraine

2 National Scientific Center, Kharkov Institute for Physics and Technology, NASU, Kharkov, Ukraine

References

[1] Lowry MB, Kiener D, LeBlanc MM, Chisholm C, Florando JN, Morris JW Jr, Minor AM. Achieving the ideal strength in annealed molybdenum nanopillars. Acta Mat. 2010;**58**: 5160-5167. DOI: 10.1016/j.actamat. 2010.05.052

[2] Bei H, Shim S, Pharr GM, George EP. Effects of pre-strain on the compressive stress–strain response of Mo-alloy single-crystal micropillars. Acta Mat. 2008;**56**:4762-4770. DOI: 10.1016/j.actamat.2008.05.030

[3] Bei H, Shim S, George EP, Miller MK, Herbert EG, Pharr GM. Compressive strengths of molybdenum alloy micro-pillars prepared using a new technique. Scr Mat. 2007;**57**:397-400. DOI: 10.1016/j.actamat.2008.05.030

[4] Shpak AP, Kotrechko SO, Mazilova TI, Mikhailovskij IM. Inherent tensile strength of molybdenum nanocrystals. Science and Technology of Advanced Materials. 2009;**10**(1–9): 045004. DOI: 10.1088/1468-6996/10/4/045004

[5] Bakai AS, Shpak AP, Wanderka N, Kotrechko SO, Mazilova TI, Mikhailovskij IM. Inherent strength of zirconium-based bulk metallic glass. Journal of Non-Crystalline Solids. 2010;**356**:1310-1314. DOI: 10.1016/j.jnoncrysol.2010.03.009

[6] Mikhailovskij IM, Sadanov EV, Kotrechko S, Ksenofontov VA, Mazilova TI. Measurement of the inherent strength of carbon atomic chains. Physical Review B. 2013;**87**(1–7):045410. DOI: 10.1103/PhysRevB.87.045410

[7] Gall K, Diao J, Dunn ML. The strength of gold nanowires. Nano Letters. 2004;**4**:2431-2436. DOI: 10.1021/nl048456s

[8] Diao J, Gall K, Dunn ML, Zimmerman JA. Atomistic simulations of the yielding of gold nanowires. Acta Mat. 2006;**54**:643-653. DOI: 10.1016/j.actamat.2005.10.008

[9] Wu HA. Molecular dynamics study on mechanics of metal nanowire. Mechanics Research Communications. 2006;**33**:9-16. DOI: 10.1016/j.mechrescom.2005.05.012

[10] Yang Z, Lu Z, Zhao YP. Atomistic simulation on size-dependent yield strength and defects evolution of metal nanowires. Comp Mat Sci. 2009;**46**:142-150. DOI: 10.1016/j.commatsci.2009.02.015

[11] Diao J, Gall K, Dunn ML. Atomistic simulation of the structure and elastic properties of gold nanowires. Journal of the Mechanics and Physics of Solids. 2004;**52**:1935-1962. DOI: 10.1016/j.jmps.2004.03.009

[12] Lao J, Tam MN, Pinisetty D, Gupta N. Molecular dynamics simulation of FCC metallic nanowires: A review. Journal of Metals. 2013;**65**:175-184. DOI: 10.1007/s11837-012-0465-3

[13] Wen YH, Zhang Y, Wang Q, Zheng JC, Zhu ZZ. Orientation-dependent mechanical properties of au nanowires. Computational Materials Science. 2010;**48**:513-519. DOI: 10.1016/j.commatsci.2010.02.015

[14] Kotrechko S, Filatov O, Ovsjannikov O. Peculiarities of plastic deformation and failure of nanoparticles of b.c.c. Transition metals. Materials Science Forum. 2007;**567–568**:65-68

[15] Kotrechko S, Ovsjannikov A. Temperature dependence of the yield stress of metallic nanosize crystals. Phil Mag. 2009;**89**:3049-3058. DOI: 10.1080/14786430903179554

[16] Wang P, Chou W, Nie A, Huang Y, Yao H, et al. Molecular dynamics simulation on deformation mechanisms in body-centered cubic molybdenum nanowires. Journal of Applied Physics. 2011;**110**(1–8):093521. DOI: 10.1063/1.3660251

[17] Sainath G, Choudhary BK. Molecular dynamics simulations on size dependent tensile deformation behaviour of [110] oriented body centred cubic ironnanowires. Mat Sci Eng A. 2015;**640**:98-105. DOI: 10.1016/j.msea.2015.05.084

[18] Kotrechko S, Ovsjannikov O, Stetsenko N, Mikhailovskij I, Mazilova T, Starostenko M. Yield strength temperature dependence of tungsten nanosized crystals: Experiment and simulation. Phil Mag. 2016;**96**:473-485. DOI: 10.1080/14786435.2016.1140913

[19] Kotrechko S, Ovsjannikov O, Mazilova T, Mikhailovskij I, Sadanov E, Stetsenko N. Inherent hydrostatic tensile strength of tungsten nanocrystals. Phil. Mag. 2017;**97**:930-943. DOI: 10.1080/14786435.2017.1285500

[20] Dutta A. Compressive deformation of Fe nanopillar at high strain rate: Modalities of dislocation dynamics. Acta Mat. 2017;**125**:219-230. DOI: 10.1016/j.actamat.2016.11.062

[21] Bin MA, Qiu-hua RAO, Yue-hui HE. Effect of crystal orientation on tensile mechanical properties of single-crystal tungsten nanowire. Transactions of the Nonferrous Metals Society of China. 2014;**24**:2904-2910. DOI: 10.1016/S1003-6326(14)63425-7

[22] Rabkin E, Nam HS, Srolovitz DJ. Atomistic simulation of the deformation of gold nanopillars. Acta Mat. 2007;**55**:2085-2099. DOI: 10.1016/j.actamat.2006.10.058

[23] Zhang L, Lu C, Kiet T, Pei L, Zhao X. Effect of stress state on deformation and fracture of nanocrystalline copper: Molecular dynamics simulation. Chinese Physics B. 2014;**23**(1–8): 098102. DOI: 10.1088/1674-1056/23/9/098102

[24] Levitas VI, Chen H, Xiong L. Triaxial-stress-induced homogeneous hysteresis-free first-order phase transformations with stable intermediate phases. PRL. 2017;**118**(1–5):025701. DOI: 10.1103/PhysRevLett.118.025701

[25] Miller MK, Cerezo A, Hetherington MG, Smith GDW. Atom Probe Field Ion Microscopy. Oxford: Oxford Science Publications—Claredon Press; 1996. p. 532

[26] Müller W, Tsong TT. Field-Ion Microscopy, Principles and Applications. New York: Elsevier; 1969

[27] Mikhailovskij IM, Wanderka N, Storizhko VE, Ksenofontov VA, Mazilova TI. A new approach for explanation of specimen rupture under high electric field. Ultramicroscopy. 2009;**109**:480-485. DOI: 10.1016/j.ultramic.2008.12.003

[28] Tsong TT. Atom-Probe Field Ion Microscopy: Field Ion Emission and Surfaces and Interfaces at Atomic Resolution. Cambridge, New York: Cambridge University Press; 1990

[29] Miller MK, Forbes RG. Atom-Probe Tomography: The Local Electrode Atom Probe. New York: Springer; 2014. DOI: 10.1007/978-1-4899-7430-3

[30] Dai X, Kong Y, Li J, Liu B. Extended Finnis–Sinclair potential for bcc and fcc metals and alloys. J Phys: Condens Mat. 2006;**18**:4527-4542. DOI: 10.1088/0953-8984/18/19/008

[31] Finnis W, Sinclair JE. A simple empirical N-body potential for transition metals. Phil Mag A. 1984;**50**:45-55. DOI: 10.1080/01418618408244210

[32] Kotrechko S, Ovsjannikov A. Temperature dependence of the yield stress of metallic nanosized crystals. Phil Mag. 2009;**89**:3049-3058. DOI: 10.1080/14786430903179554

[33] Roundy D, Krenn CR, Cohen ML, Morris JW Jr. The ideal strength of tungsten. Phil Mag A. 2001;**81**:1725-1747. DOI: 10.1080/01418610108216634

[34] Weidong L, Roundy D, Cohen ML, Morris JW Jr. Ideal strength of bcc molybdenum and niobium. Physical Review B. 2002;**66**:094110. DOI: 10.1103/PhysRevB.66.094110

[35] Clatterbuck DM, Chrzan DC, Morris JW Jr. The ideal strength of iron in tension and shear. Acta Mat. 2003;**51**:2271-2283. DOI: 10.1016/S1359-6454(03)00033-8

[36] Diao J, Gall K, Dunn ML. Yield strength asymmetry in metal nanowires. Nano Letters. 2004;**4**:1863-1867. DOI: 10.1021/nl0489992

[37] Kotrechko S, Timoshevskii A, Mikhailovskij I, Mazilova T, Stetsenko N, Ovsijannikov O, Lidych V. Atomic mechanisms governing upper limit on the strength of nanosized crystals. Engineering Fracture Mechanics. 2015;**150**:184-196. DOI: 10.1016/j.engfracmech.2015.03.025

[38] Leibfried G. Gittertherie der mechanischer und thermischen eigenschaften der kristalle Handbuch der physic, Band VII Teil 2. Berlin: Springer-verlag; 1955

[39] Al-Rawi AN, Kara A, Rahman TS. Comparative study of anharmonicity: Ni.111., Cu.111., and Ag.111. Physical Review B. 2002;**66**(1–10):165439. DOI: 10.1103/PhysRevB.66.165439

[40] Kotrechko SA, Filatov AV, Ovsjannikov AV. Molecular dynamics simulation of deformation and failure of nanocrystals of bcc metals. Theoretical and Applied Fracture Mechanics. 2006;**45**:92-99. DOI: 10.1016/j.tafmec.2006.02.002

[41] Šob M, Wang LG, Vitek V. The role of higher-symmetry phases in anisotropy of theoretical tensile strength of metals and intermetallics. Phil Mag B. 1998;**78**:653-658. DOI: 10.1080/13642819808206773

[42] Černý M, Řehák P, Pokluda J. The origin of lattice instability in bcc tungsten under triaxial loading. Phil Mag. 2017;**97**:2971-2984. DOI: 10.1080/14786435.2017.1363424

[43] Kim JY, Jang DC, Greer JR. Tensile and compressive behavior of tungsten, molybdenum, tantalum and niobium at the nanoscale. Acta Mat. 2010;**58**:2355-2363. DOI: 10.1016/j.actamat.2009.12.022

[44] Kim JY, Jang DC, Greer JR. Insight into the deformation behavior of niobium single crystals under uniaxial compression and tension at the nanoscale. Scripta Materialia. 2009;**61**:300-303. DOI: 10.1016/j.scriptamat.2009.04.012